Acta Biomaterialia 170 (2023) 507–518

Contents lists available at ScienceDirect

Acta Biomaterialia

journal homepage: www.elsevier.com/locate/actbio

Full length article

Brain Stiffness Follows Cuprizone-Induced Variations in Local Myelin Content

Xuesong Zhang, Johannes Weickenmeier*

Department of Mechanical Engineering, Stevens Institute of Technology, Hoboken, NJ 07030 United States

ARTICLE INFO

Article history:
Received 25 January 2023
Revised 8 August 2023
Accepted 17 August 2023
Available online 1 September 2023

Keywords:
myelin
tissue stiffness
microstructure
corpus callosum
cingulum
cortex
demyelination
cuprizone model
indentation

ABSTRACT

Brain maturation and neurological diseases are intricately linked to microstructural changes that inherently affect the brain's mechanical behavior. Animal models are frequently used to explore relative brain stiffness changes as a function of underlying microstructure. Here, we are using the cuprizone mouse model to study indentation-derived stiffness changes resulting from acute and chronic demyelination during a 15-week observation period. We focus on the corpus callosum, cingulum, and cortex which undergo different degrees of de- and remyelination and, therefore, result in region-specific stiffness changes. Mean stiffness of the corpus callosum starts at 1.1 ± 0.3 kPa in untreated mice, then cuprizone treatment causes stiffness to drop to 0.6 ± 0.1 kPa by week 3, temporarily increase to 0.9 ± 0.3 kPa by week 6, and ultimately stabilize around 0.7 ± 0.1 kPa by week 9 for the rest of the observation period. The cingulum starts at 3.2 ± 0.9 kPa, then drops to 1.6 ± 0.4 kPa by week 3, and then gradually stabilizes around 1.4 ± 0.3 kPa by week 9. Cortical stiffness exhibits less stiffness variations overall; it starts at 4.2 ± 1.3 kPa, drops to 2.4 ± 0.6 kPa by week 3, and stabilizes around 2.7 ± 0.9 kPa by week 6. We also assess the impact of tissue fixation on indentation-based mechanical tissue characterization. On the one hand, fixation drastically increases untreated mean tissue stiffness by a factor of 3.3 for the corpus callosum, 2.9 for the cingulum, and 3.6 for the cortex; on the other hand, fixation influences interregional stiffness ratios during demyelination, thus suggesting that fixation affects individual brain tissues differently. Lastly, we determine the spatial correlation between stiffness measurements and myelin density and observe a region-specific proportionality between myelin content and tissue stiffness.

Statement of significance

Despite extensive work, the relationship between microstructure and mechanical behavior in the brain remains mostly unknown. Additionally, the existing variation of measurement results reported in literature requires in depth investigation of the impact of individual cell and protein populations on tissue stiffness and interregional stiffness ratios. Here, we used microindentation measurements to show that brain stiffness changes with myelin density in the cuprizone-based demyelination mouse model. Moreover, we explored the impact of tissue fixation prior to mechanical characterization because of conflicting results reported in literature. We observe that fixation has a distinctly different impact on our three regions of interest, thus causing region-specific tissue stiffening and, more importantly, changing interregional stiffness ratios.

1. Introduction

Brain maturation and many neurological diseases are characterized by microstructural changes that inherently alter the tissues' mechanical behavior [1–5]. Extensive work has gone into the mechanical characterization of brain tissues and evaluation of spatial relationships between microstructure and mechanical properties [6–9]. Systematic study of mechanobiological changes in neurological diseases is particularly challenging, however, due to the tissues' inaccessibility for mechanical characterization. Therefore, animal models which closely mimic human neuropathology have proven useful to uncover many critical mechanobiological mechanisms of disease. At the same time, distinct differences in mi-

* Corresponding author.
E-mail address: johannes.weickenmeier@stevens.edu (J. Weickenmeier).

https://doi.org/10.1016/j.actbio.2023.08.033
1742-7061/

crostructural composition, size, metabolic activity, and lifetime of animal brains in comparison to human brains, pose limitations on projecting animal model-derived mechanical properties onto the human brain [10–12]. Nonetheless, animal models allow us to explore relative brain stiffness changes as a function of underlying microstructure. Previous work has used indentation [9,13–15], rheology [16], and magnetic resonance elastography [11,17,18] to evaluate animal brain properties as a surrogate for human brain tissue in diseases such as multiple sclerosis [15,19,20], Alzheimer's disease [1,21], and age [4,9], amongst others. All of these diseases are associated with microstructural degeneration that alter the tissues' mechanical properties as well as function. In many instances, however, the mechanical microenvironment plays a critical role in enabling or preventing the brain's ability to repair disease-induced damage [22,23]. Since demyelination is a common pathology in aging and neurodegeneration, it is worthwhile exploring the impact of myelin content variations on tissue stiffness in distinctly different brain regions such as the corpus callosum, cingulum, and cortex.

Amongst the most prominent cell and protein populations in the mouse brain, myelin content has been shown to correlate with brain stiffness [14,15,17]. Myelin plays a critical role during development while the brain's functional network is formed [24]. It is also affected by demyelinating diseases that are associated with progressive loss of cognitive function [25]. The cuprizone mouse model is the most commonly used surrogate to investigate disease-related brain changes such as lesion formation and spontaneous remyelination [26,27]. In mice, 0.2% cuprizone treatment for up to 6 weeks, causes metabolic stress which leads to comprehensive demyelination, depletion of oligodendrocyte progenitor cells, and triggers neuroinflammation associated with astrogliosis and microgliosis [28]. Cuprizone treatment beyond 6 weeks has shown to include a brief period of spontaneous, albeit partial, white matter remyelination despite continued toxin exposure. In the long-term, however, extending cuprizone treatment to 12 weeks and beyond, results in multiple failed cycles of remyelination and ultimately causes irreversible chronic demyelination [15]. Interestingly, if toxin is withdrawn, white and gray matter tissue tends to show spontaneous remyelination and can even achieve near full recovery [29].

The primary objective of the present work is to assess brain tissue stiffness variations over a continuous 15-week cuprizone treatment period to determine if mechanical properties follow spatiotemporal myelin content changes. We quantify the temporal stiffness changes resulting from initial demyelination during the first 5 weeks, the subsequent remyelination by week 6 (irrespective of continuous cuprizone treatment), and the subsequent chronic demyelination observed during the remaining weeks. We focus on quantifying the temporal stiffness variations observed between the two extreme groups, i.e., untreated and chronically treated mice, and providing a region-specific relationship between tissue stiffness and myelin content. We derived tissue stiffness from microindentation measurements based on a minimum of 72 measurements in the corpus callosum and 36 measurements in the cingulum and cortex, respectively, for each animal. We focus on these regions, because the gray-white matter stiffness ratio plays a critical role in many computational models that try to predict age- and disease-related biomechanical brain behavior [30–33]. We also investigated the impact of tissue fixation on relative interregional stiffness ratios because previous works have used both fresh and fixed tissues with conflicting findings. To assess microstructure, we used histological staining and quantified myelin fractions from microscopy images. A better understanding of the spatiotemporal correlation between local stiffness and myelin density is particularly useful for estimating mechanical tissue changes in many neurological diseases such as multiple sclerosis and neurodegenerative diseases. Novel magnetic resonance imaging sequences are able to quantify in vivo microstructural deterioration related to demyelination at significantly higher resolution in comparison to direct stiffness measurements based on magnetic resonance elastography [34–36]. The work presented here, will help develop new methods to infer tissue stiffness changes and the level of tissue damage from in vivo brain imaging.

2. Methods

All research and animal care procedures were approved by the Institutional Review Board at Stevens Institute of Technology under animal protocol 2019-004(AP) and performed according to international guidelines on the use of laboratory animals.

2.1. Cuprizone mouse model to study demyelination

To systematically study brain stiffness changes on the basis of varying degrees of axon myelination, we utilize the cuprizone mouse model. By substituting regular mouse diet with cuprizone treated chow, we can induce varying degrees of white and gray matter myelination based on exposure time. In this study, we obtained 50 8-week-old female C57BL/6 mice from Jackson Laboratory and divided them into two groups: an untreated group with 17 mice to serve as controls and a group with 33 animals that were placed on a cuprizone diet. Mice were caged in groups of 3 or 4 animals in a climate-controlled room. They received water and chow ad libitum. Untreated mice received regular chow (Envigo, Indianapolis, IN) for up to 3 and 6 weeks, respectively. Treated mice received 0.2% cuprizone chow (Envigo, Indianapolis, IN) without interruption for 3, 6, 9, 12, and 15 weeks, respectively. Figure 1 shows the timeline of our study. For mechanical testing, we harvested untreated mice at week 0 ($n = 5$), week 3 ($n = 5$), and week 6 ($n = 7$) to assess brain stiffness variations with age. We harvested cuprizone-treated mice at week 3 ($n = 6$), week 6 ($n = 6$), week 9 ($n = 6$), week 12 ($n = 7$), and week 15 ($n = 8$). To assess differences between fresh and fixed tissue stiffness variations, we harvested additional untreated mice ($n = 5$) and treated mice ($n = 6$) after 6 weeks of observation. For both groups, we prepare a sample per brain, fix it for 24 hours and then perform mechanical testing, as outlined in Section 2.3. We harvested $n = 3$ mice at weeks 0 (baseline), 3, 4, 5, and 6, respectively, for histochemical analysis to quantify microstructural changes and variations in myelination as described in Section 2.5.

2.2. Sample preparation

All samples were prepared the same way. Mice were sacrificed via cervical dislocation. Their brains were subsequently harvested and transferred to a custom-built cutting mold to remove the cerebellum as shown in Fig. 2a/b. The flat surface was then glued onto the VT-1200S vibratome disc (Leica Biosystems, Buffalo Grove, IL) using Gorilla Super Glue (Gorilla Inc., Cincinnati, Ohio) which was then placed in a fluid chamber filled with phosphate buffered saline (PBS) at $22 \pm 1\,^{\circ}C$, see Fig. 2c. We used the vibratome to cut a 1 mm thick coronal slice at 0.7 mm Bregma. We used a vibratome blade speed of 0.1 mm/s, vibration amplitude of 1 mm, and vibration frequency of 85 Hz. The caudal-facing side of the slice was then glued to the bottom of a 35 mm diameter petri dish (Benz Microscope Optics Center, Inc., Washtenaw County, Michigan) using Gorilla Super Glue and washed with PBS, as shown in Fig. 2d. Prior to mechanical testing, samples were fully submerged in Opti-Free contact lens solution (Alcon, Fort Worth, Texas). We used contact lens solution because it drastically lowers the interfacial tension between fluid and indenter and thereby reduces the

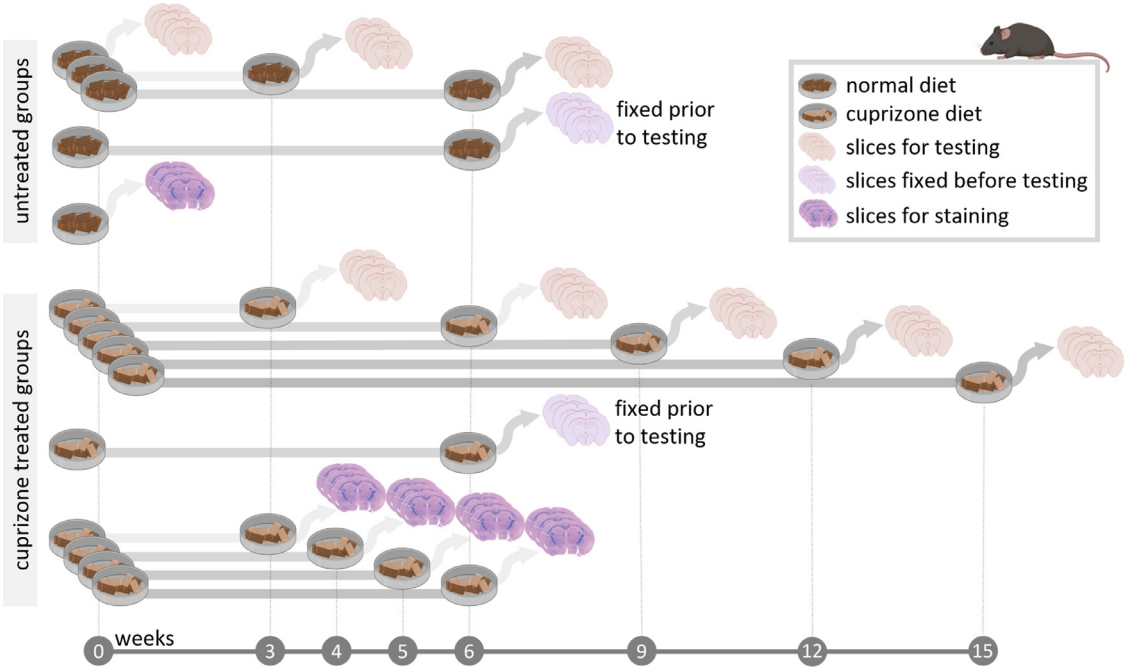

Fig. 1. Mouse feeding and sample preparation plan. We distinguish between healthy controls, harvested after 0, 3, and 6 weeks and cuprizone treated groups that are harvested at 0, 3, 6, 9, 12, and 15 weeks. We prepare samples for tissue staining at 0 weeks to establish the baseline and after 3, 4, 5, and 6 weeks of cuprizone treatment. Samples that were fixed prior to indentation testing we harvested after 6 weeks of regular chow and 6 weeks of cuprizone treatment, respectively.

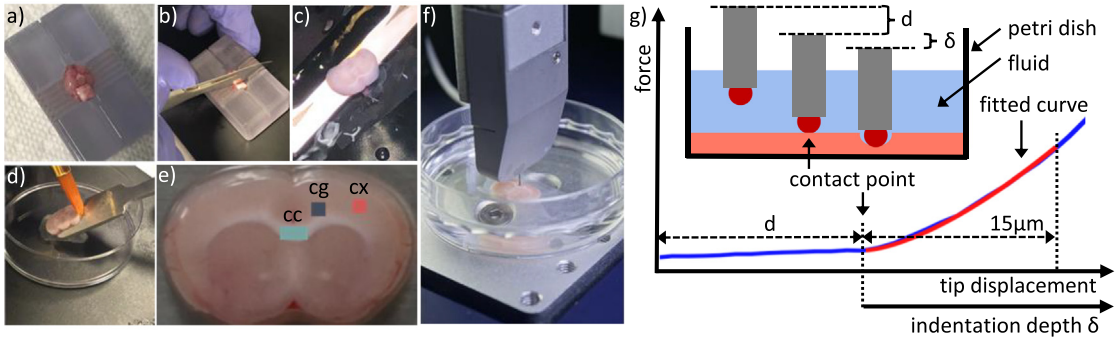

Fig. 2. Indentation procedure: we harvest the brain, a) place the brain in a tissue slicer, b) cut away the brainstem, c) transfer the sample to a vibratome to cut a 1000 µm thick slice, d) glue the sample into a petri dish, and e) identify the regions of interest for indentation testing, i.e., the corpus callosum (cc, green box), cingulum (cg), and cortex (cx, red box), f) finally we perform grid measurements in each region of interest using our microindentation machine. Per our indentation protocol, g) we start each measurement out of contact, approach the sample, and upon detecting the contact point, prescribe an indentation depth δ of 15 µm. We record tip reaction force during the entire process and ultimately determine tissue stiffness by fitting the Sneddon model to the force-displacement data as shown in red.

drag forces on the tip as we indent the brain. All mechanical indentation tests on each slice were performed at (22 ± 1 °C) and completed within 4 hours of death.

To obtain fixed samples for mechanical testing, a 1 mm thick coronal slice was harvested from each brain at 0.7 mm Bregma and transferred to a test tube with 10 ml 10% neutral buffered formalin for fixation. After 24 hours of fixation at 22 ± 1 °C , the caudal-facing side of the fixed slices were glued to the bottom of a 35 mm diameter petri dish, washed with PBS, and subsequently submerged in contact lens solution prior to mechanical testing.

2.3. Indentation protocol

We tested three characteristic brain regions in all mice: the corpus callosum (cc), cingulum (cg), and cortex (cx). In each region of interest, we performed grid measurements. In the corpus callosum, we performed 12 x 6 measurements with 50 µm spacing for a total of n = 72 measurements covering an area of 600 µm by 300 µm. In both the cingulum and cortex, we performed 6 x 6 measurements with 50 µm inter-measurement spacing for a total of n = 36 measurements covering an area of 300 µm by 300 µm, see Fig. 2e. It is important to note, that our grid size of 300 µm by 300 µm might exceed the actual size of the cingulum which is up to 400 µm wide [37] and may laterally extend into the cortical layer by up to one column of measurements. We accept this slight overlap with the cortex as this anatomical region represents a transition zone from the corpus callosum to the cortex. Once samples were placed inside the indentation machine, we used the integrated microscope to localize the desired test locations. Specifically, the symmetry axis of the coronal slice marks the the center of the corpus callosum grid. We then identify the bottom left corner of the cingulum grid such that we do not overlap with the corpus callosum. The position of the cortical grid is defined relative to the top right corner of the corpus callosum grid with a vertical offset of 600 µm and lateral offset of 1200 µm. All measurements were conducted using our FT-MTA03 Micromechanical Testing System (FemtoTools AG, Schlieren, Switzerland) equipped with an FT-S200 Micro-Force Sensing Probe (FemtoTools AG, Schlieren,

Switzerland) which has a force range of -200 µN to 200 µN and 0.0005 µN resolution at 10 Hz. We customized our probe by gluing a 50 µm diameter polystyrene microsphere (Alpha Nanotech, Research Triangle, NC) to its tip. We placed each petri dish in the indentation machine, as shown in Fig. 2f.

Before starting grid measurements, the machine automatically identifies the sample surface by lowering the probe at a speed of 100 µm/s. When an indentation force of 3 µN is detected, the sensor retracts by 40 μm and saves this vertical position as the starting height for all subsequent grid measurements. We use this approach because of the slightly uneven sample surface. We then start the automatically controlled grid measurements. For each grid point, the machine lowers the probe by 10 µm/s until a force threshold of 0.3 µN is reached upon which the machine switches to a displacement-controlled indentation test and indents the sample by an additional 15 µm, see Fig. 2g. Following maximum indentation, the probe returns to the vertical starting position and moves to the next grid point for another measurement. The force threshold is chosen this high to avoid a switch to the displacement driven part before the indenter is in contact with the sample. During the automated grid tests, we cannot afford to trigger incomplete measurements too often. During post-processing, we discard those measurements from further consideration. Force and tip displacement data are sampled at 40 Hz.

After collecting all data, we use a custom python code to retrospectively determine the contact point between indenter and sample which occurs at some point before the force threshold. The ultrasoft properties of the brain tissue present a challenge for identifying the exact contact point which is characterized by a gradual change in the slope of the force-displacement curve, as shown in Fig. 2g. Our algorithm first identifies the point of maximum indentation force. From there, it uses a moving window with the ten previous measurement points and determines the slope of a linear fit through the displacement data. We iteratively move this data window in reverse loading direction until the slope decreases to a minimum threshold of $\kappa = 0.008$ µN/µm which we determined during the protocol development phase. Once we reach our threshold we define the minimum displacement value in the current data window as our contact point. We subsequently clip the force-tip displacement data before the contact point and above 15 µm indentation depth for stiffness identification. This approach ensures that we only analyze the tissue response for up to about 15.5% strain for which the Sneddon model is a good approximation of the force-displacement data [38].

2.4. Stiffness identification

We determine the apparent elastic modulus E, based on the Sneddon model for spherical indentation [38] given by equations

$$F = \frac{E}{1-\nu^2}\left[\frac{a^2+R_s^2}{2}\ln\frac{R_s+a}{R_s-a} - aR_s\right] \text{ with } \delta = \frac{a}{2}\ln\left[\frac{R_s+a}{R_s-a}\right]. \tag{1}$$

Here, F is the indentation force, R_s is the indenter's spherical tip radius that is 25 μm and a is the contact radius. We follow the common assumption that brain tissue may be treated as incompressible, i.e., Poisson's ratio $\nu = 0.5$. Contact radius a is related to the indenter's spherical tip radius and indentation depth δ measured during each indentation with $\delta_{\max} = 15$ µm. For each measurement point, we take the displacement data, derive the corresponding contact radii, and fit the force data by iterating on the apparent elastic modulus. Specifically, we use the nonlinear least squares implementation of the SciPy library in python which minimizes the residual sum of squares, *RSS*, given by $RSS = \sum_{i=1}^{n}\left(y_i - f(x_i)\right)^2$, where y_i is our experimental force data and $f(x_i)$ is the prediction from the Sneddon model, see Eq. 1. For each region, we store each grid point's apparent elastic modulus for our subsequent statistical analysis.

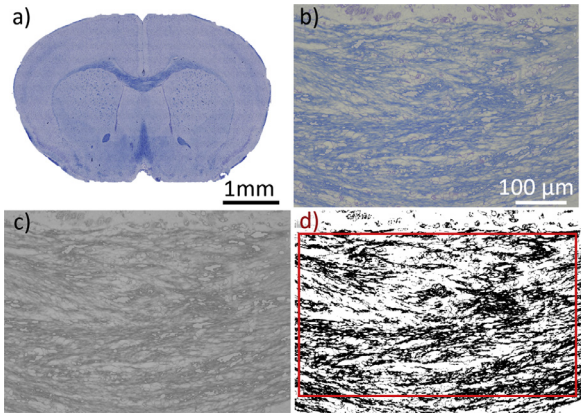

Fig. 3. Microstructural assessment. a) We stain formaldehyde-fixed whole brain cortical slices with luxol fast blue and counterstain cresyl violet such that myelin appears blue and nissl substance appears purple. b) We then obtain 20x magnified images of the corpus callosum (shown here after nuclei were removed), cingulum, and cortex, and apply several image processing steps to determine myelin fraction. To that end, c) we convert them to a grayscale image and d) binarize them based on an intensity value of 155. The red box shows the region used to quantify myelin fraction.

2.5. Histology and image analysis

We use histology to quantify the microscopic anatomy at our indentation sites. Tissue slices harvested for staining were fixed in 10% neutral buffered formalin for 24 hours at 22 ± 1 °C . Afterwards, slices were washed with PBS, dehydrated with ethanol, and cleared using xylene. Slices were then embedded in paraffin for sectioning. We cut 5 µm thick slices using a microtome (RM2135, Leica Biosystems, Buffalo Grove, IL) and transferred them to a glass side. Among the possible stains to measure myelin content, including myelin basic protein, myelin-associated glycoprotein, and proteolipid protein immunostaining, we selected luxol fast blue (StatLab Medical Products, McKinney, TX) [39]. The copper phthalocyanine chromogen in luxol fast blue is attracted to the bases in the lipoproteins of the myelin sheath [40]. We then counterstained with cresyl violet (StatLab Medical Products, McKinney, TX) such that myelin appears in blue, neuropil in pink, and nerve cells in purple, as shown in Fig. 3a. Although luxol fast blue is widely used to quantify the changes of myelin content, it is not clear if the change is caused by a variation of myelin concentration or axon density, or both [41].

According to our staining protocol, we deparaffinize slices with xylene and rinse them with ethanol and deionized water. They are then submerged in preheated luxol fast blue solution for 1 hour at 60 °C, washed with ethanol and deionized water, and subsequently submerged in cresyl echt violet solution for 10 minutes at 22 ± 1 °C . Finally, slices were dehydrated by ethanol, cleared by xylene, and mounted using permanent mounting media (Electron Microscopy Sciences, Hatfield, PA). We prepared a total of 14 histology-stained slices and used light microscope (Eclipse Ci-L, Nikon Instruments Inc., Melville, NY) to create digital copies with a 5.9 megapixel camera (DS-Fi3, Nikon Instruments Inc., Melville, NY), see Fig. 3a. All images were subsequently post-processed with our custom-code to quantify myelin content. We first remove cell nuclei by thresholding the green color channel (index up to 255) based on a value of 85 for the corpus callosum, 95 for cingulum, and 145 for the cortex. Respective pixels were set to the

Table 1
Summary of our indentation measurements in **fresh** mouse brain tissue, i.e, the corpus callosum (cc), cingulum (cg), and the cortex (cx). We differentiate between fresh untreated and fresh treated mice that we sacrificed at various time points. We report number of mice, mean stiffness and standard deviation of all measurements per location, and number of measurements per location. See Fig. S1 for each individual measurement.

	week	# mice	region	mean [kPa]	SD [kPa]	n
	0	5	cc	1.1	0.3	323
			cg	3.2	0.8	180
			cx	4.1	0.9	180
untreated	3	5	cc	1.1	0.2	299
			cg	3.7	1.0	174
			cx	4.4	1.0	179
	6	7	cc	1.2	0.3	302
			cg	2.9	0.8	244
			cx	4.2	1.8	174
	3	6	cc	0.6	0.1	403
			cg	1.6	0.4	205
			cx	2.4	0.6	216
	6	6	cc	0.9	0.3	380
			cg	1.9	0.6	216
			cx	2.7	0.9	216
treated	9	6	cc	0.7	0.1	359
			cg	1.4	0.3	208
			cx	2.5	0.5	204
	12	7	cc	0.7	0.2	427
			cg	1.2	0.3	250
			cx	2.2	0.4	252
	15	8	cc	0.8	0.1	535
			cg	1.8	0.6	281
			cx	3.0	0.7	288

Table 2
Summary of our indentation measurements in **fixed** mouse brain tissue, i.e., the corpus callosum (cc), cingulum (cg), and the cortex (cx). We differentiate between fixed untreated and fixed treated mice that we sacrificed at various time points. We report number of mice, mean stiffness and standard deviation of all measurements per location, and number of measurements per location. See Fig. S2 for each individual measurement.

	week	# mice	region	mean [kPa]	SD [kPa]	n
untreated	6	5	cc	4.0	1.6	329
			cg	8.6	4.0	180
			cx	15.3	6.3	124
treated	6	6	cc	4.1	1.8	355
			cg	5.3	2.2	187
			cx	8.6	6.3	150

background color, see Fig. 3b. We then isolate myelin by converting each image to a grayscale image, see Fig. 3c, and binarize the new images based on an intensity value of 155, see Fig. 3d [41]. We then identified our three indentation sites and created a copy at twenty-times magnification for each location. As shown in Fig. 3d, this approach accurately differentiates between myelin and all other constituents. We ultimately define myelin content as the fraction of black pixels over all pixels.

2.6. Statistical analysis

We conducted the statistical analyses in R (Version 4.1.2) where statistical significance was defined by $p < 0.05$. For all data, we used a linear mixed model as implemented in the R package *afex*. All post-hoc analyses were conducted using Tukey tests. In this manuscript, we report data as mean with standard deviation, see Tables 1-2, although all statistical analyses are based on including every single measurement point to account for intra- and inter-animal variance. In the supplementary materials, we report all individual stiffness measurements as swarm plots where measurements from the same animal are in the same color. We evaluated the effect of tissue fixation on interregional stiffness ratios using a bootstrapping approach with 1000 iterations. For each iteration and animal, we randomly sampled 10 stiffness measurements from each of the three regions. We then computed pairwise ratios, i.e., cortex/corpus callosum, cingulum/corpus callosum, and cortex/cingulum, and store the three respective mean values for each ratio. We then construct a histogram for each animal and ratio which are shown in Fig. S3 in the supplementary materials. Since all histograms follow a normal distribution, we report their mean and standard deviation in Table 3 and use mean values for subsequent analyses in Section 3.2.

Table 3
Summary of interregional stiffness ratios derived from our bootstrapping approach. For each animal we sampled 1000 data sets of 10 randomly selected points, compute 10 stiffness ratios between the cortex and corpus callosum (cx/cc), cingulum and corpus callosum (cg/cc), and cortex and cingulum (cx/cg), respectively, and constructed the corresponding spatial distributions for each ratio, see Fig. S3. Here, we calculate the mean of each animal's distribution and report the mean and standard deviation for each group and region.

	week	# mice	ratio	mean [-]	SD [-]	n
fresh untreated	6	7	cx/cc	3.9	1.2	1000
			cg/cc	2.7	0.6	1000
			cx/cg	1.6	0.7	1000
fresh treated	6	6	cx/cc	3.3	1.1	1000
			cg/cc	2.2	0.5	1000
			cx/cg	1.5	0.2	1000
fixed untreated	6	5	cx/cc	4.1	1.1	1000
			cg/cc	2.4	0.6	1000
			cx/cg	2.0	0.4	1000
fixed treated	6	6	cx/cc	2.1	0.8	1000
			cg/cc	1.5	0.4	1000
			cx/cg	1.5	0.5	1000

3. Results

3.1. Regional brain stiffness variations

Figure 4 shows a summary of all measurements performed in fresh tissue samples including untreated mice (Fig. 4a/c/e) and treated mice (Fig. 4b/d/f). We report the mean stiffness of each animal and region to visualize the effect of age and cuprizone treatment duration on tissue stiffness. However, our statistical analysis uses linear mixed models that fit every single measurement in order to properly account for intra- and inter-mouse variations. We show every individual measurement point in Fig. S1 in the supplementary materials where measurements from the same animal are in the same color. In untreated mice, mean stiffness and standard deviation in the corpus callosum is 1.1 ± 0.3 kPa, 1.1 ± 0.2 kPa, and 1.2 ± 0.3 kPa for weeks 0, 3, and 6, respectively; for the cingulum, these values are 3.2 ± 0.8 kPa, $3.7,\pm 1.0$ kPa, and 2.9 ± 0.8 kPa, respectively; and for the cortex, they are 4.1 ± 0.9 kPa, 4.4 ± 1.0 kPa, and 4.2 ± 1.8 kPa, respectively. Cuprizone treatment generally induces tissue softening in all three subregions. In the corpus callosum, stiffness decreases from 1.1 ± 0.3 kPa in untreated mice to 0.6 ± 0.1 kPa at week 3; stiffness then temporarily increases by 50% to 0.9 ± 0.3 kPa at week 6; it then decreases again to 0.7 ± 0.1 kPa by week 9 and maintains a similar mean value for weeks 12 (0.7 ± 0.2 kPa) and 15 (0.8 ± 0.1 kPa). A similar trend is observed for the cingulum for which stiffness drops from 3.2 ± 0.9 kPa in untreated mice to 1.6 ± 0.4 kPa at week 3; it then increases to 1.9 ± 0.6 kPa at week 6 and subsequently drops to 1.4 ± 0.3 kPa, 1.2 ± 0.3 kPa, and 1.8 ± 0.6 kPa at weeks 9, 12, and 15, respectively. Cortical stiffness exhibits less stiffness

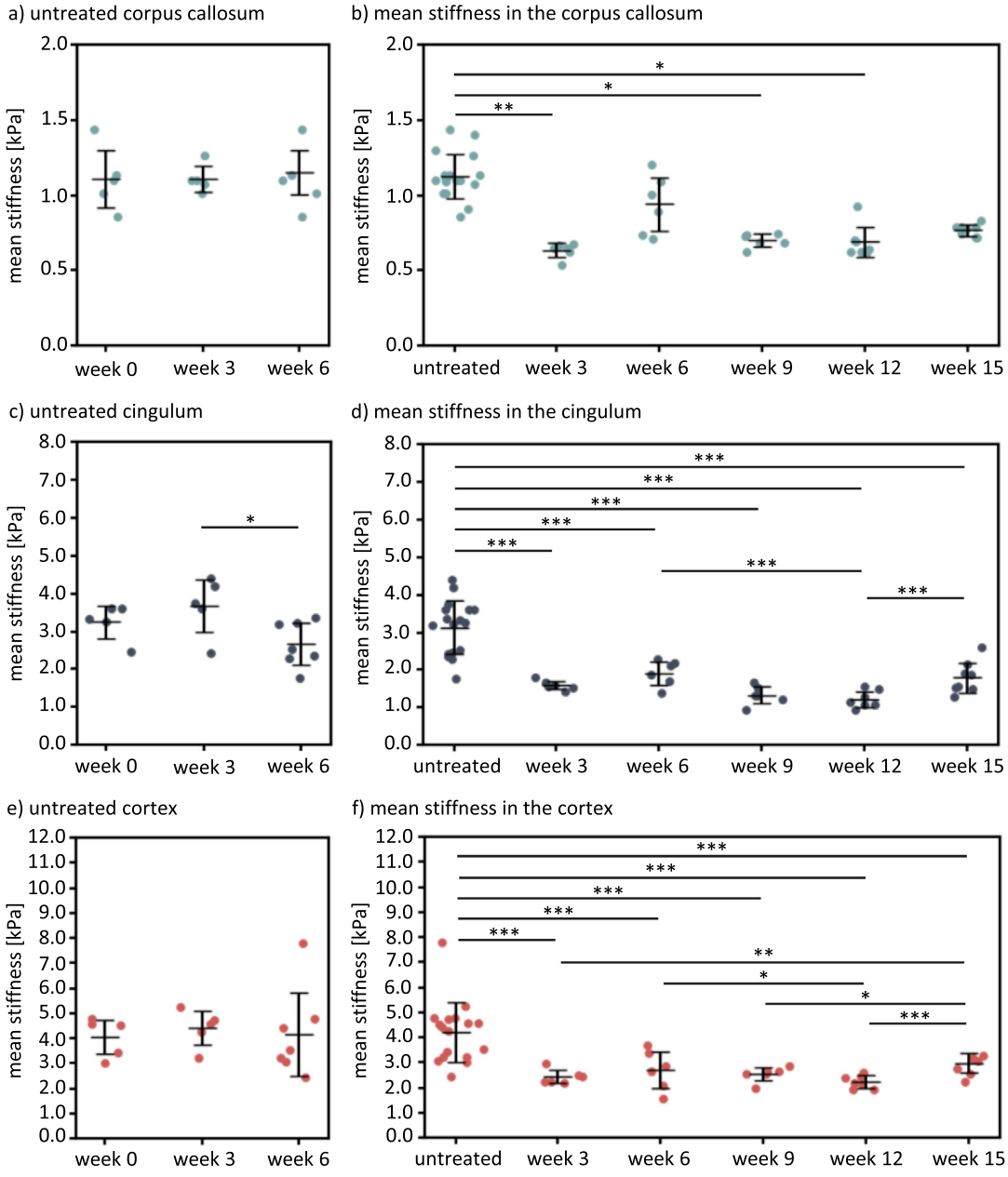

Fig. 4. Summary of all stiffness measurements using fresh samples in the form of mean stiffness per animal and region. We also indicate mean stiffness and standard deviation across all measurements (black markers). We measured untreated mouse brain stiffness at 0, 3, and 6 weeks in the a) corpus callosum, c) cingulum, and e) cortex. We also measured treated mouse brain stiffness after 3, 6, 9, 12, and 15 weeks of uninterrupted cuprizone treatment in the b) corpus callosum, d) cingulum, and f) cortex. Since no statistical difference is observed in untreated groups, except for the cingulum between weeks 3 and 6, we compare treated mice against all untreated data. We determine statistical significance between groups using Tukey post-hoc multiple comparison and report p-values as *: $p < 0.05$, **: $p < 0.01$, and ***: $p < 0.001$.

variations overall. It initially drops from 4.2 ± 1.3 kPa in untreated mice to 2.4 ± 0.6 kPa at week 3. In subsequent weeks mean stiffness remains stable with 2.7 ± 0.9 kPa, 2.5 ± 0.5 kPa, 2.2 ± 0.4 kPa, and 3.0 ± 0.7 kPa at weeks 6 through 15, respectively.

In summary, untreated mice show a statistically significant difference between regions ($p < 0.001$) but no statistically significant difference between observation period. Only the cingulum is statistically different between weeks 3 and 6 ($p = 0.011$). Cuprizone treatment, however, has a significant impact on all three regions. Especially the cingulum and cortex show significant differences compared against untreated mice irrespective of treatment duration (most p-values <0.001, see Fig. 4). The corpus callosum shows major softening by week 3 ($p = 0.006$), recovers stiffness due to temporary remyelination with no statistical significant difference compared to untreated mice, but then softens again during subsequent weeks ($p = 0.021$ and $p = 0.029$ for weeks 9 and 12, respectively).

3.2. Differences between fresh and fixed brain stiffness

Figure 5 summarizes our data investigating the differences between fresh and fixed samples. We show mean stiffness for each animal and region. Fig. S2 in the supplementary materials shows every individual measurement where measurements from the same animal are in the same color. Fig. 5a) compares 6-week

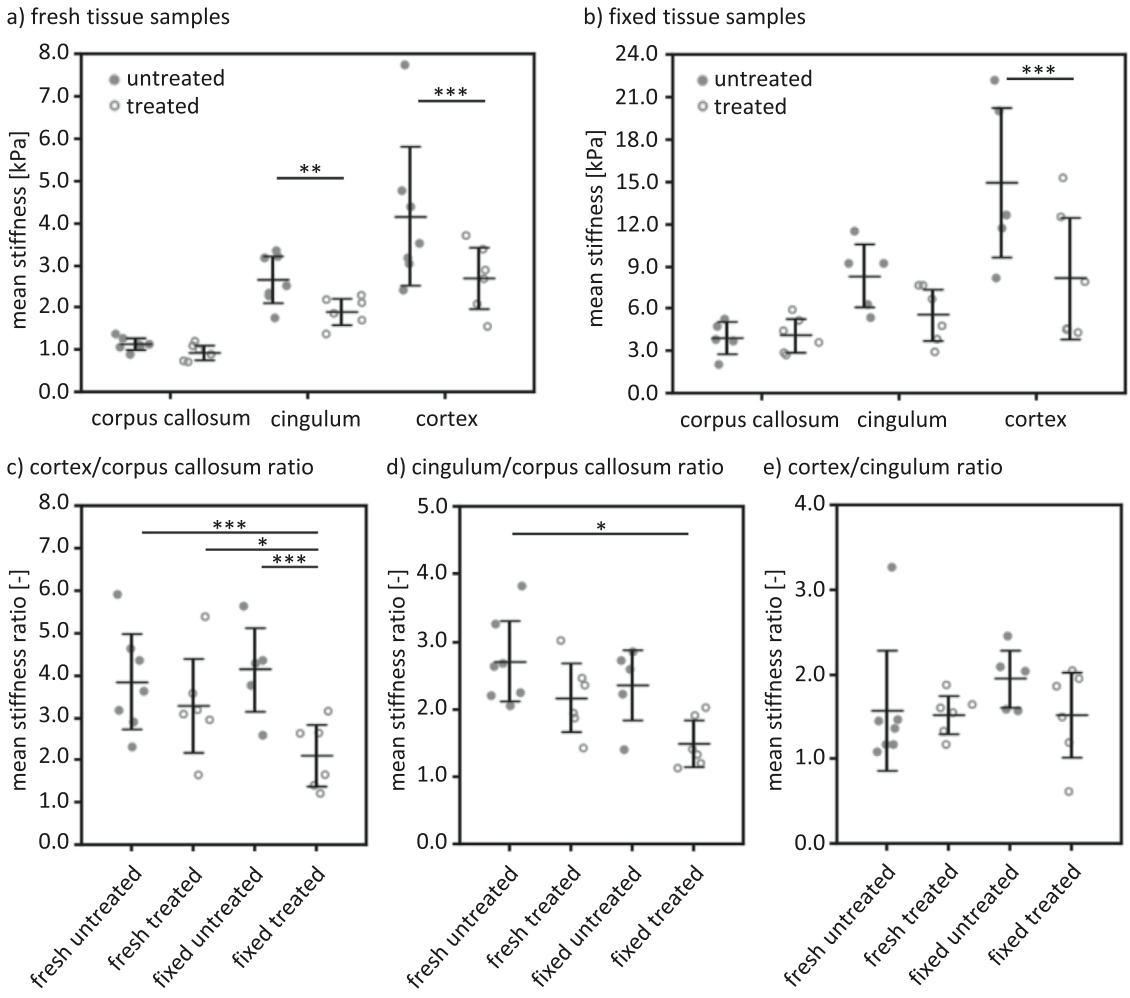

Fig. 5. Summary of measurements in 6-week old a) fresh and b) fixed untreated and treated mice. We use bootstrapping to compute a statistical distribution of the stiffness ratio between c) cortex and corpus callosum, d) cingulum and corpus callosum, and e) cortex and cingulum. Here, we report the mean ratio from each animal. We compute stiffness ratios for each of the four groups: fresh untreated, fresh treated, fixed untreated, and fixed treated mice, respectively. Black markers indicate mean and standard deviation of all data points for stiffness (a/b) and stiffness ratio (d-e), respectively. We determine statistical significance between groups using Tukey post hoc multiple comparison and report p-values as *: $p < 0.05$, **: $p < 0.01$, and ***: $p < 0.001$.

untreated data with 6-week treated stiffness in the corpus callosum, cingulum, and cortex, respectively. Fig. 5b) shows the same data for fixed tissue. For untreated mice, fixed sample stiffnesses are 4.0 ± 1.6 kPa in the corpus callosum, 8.6 ± 4.0 kPa in the cingulum, and 15.3 ± 6.3 kPa in the cortex; fixed treated sample stiffnesses are 4.1 ± 1.8 kPa in the corpus callosum, 5.3 ± 2.2 kPa in the cingulum, and 8.6 ± 6.3 kPa in the cortex. Based on these measurements, untreated fixed corpus callosum is 3.3 times, fixed cingulum is 2.9 times, and fixed cortex is 3.6 times stiffer than fresh control samples from these regions. For treated mice, fixed samples from the corpus callosum are 4.6 times, from the cingulum are 2.8 times, and from the cortex are 3.2 times stiffer than fresh samples from respective regions. In Figs. 5c-e) we report the computed stiffness ratios between the cortex and corpus callosum, cingulum and corpus callosum, and the cortex and cingulum, respectively. More specifically, we compare fresh untreated, fresh treated, fixed untreated, and fixed treated to assess if treatment and fixation influence each other. Interestingly, we observe that the cortex/corpus callosum stiffness ratio in fixed treated mice is different from fresh untreated ($p < 0.001$), fresh treated ($p = 0.048$), and fixed untreated samples ($p < 0.001$). The only other significant difference is measured for the ratio between cingulum and corpus callosum using fresh untreated and fixed treated samples ($p = 0.032$).

3.3. Correlation between myelin content and tissue stiffness

Figure 6 shows representative microscopy images of the corpus callosum, cingulum, and cortex at a) 10 times and b) 20 times magnification at weeks 0 (untreated), 4 (treated), and 6 (treated), respectively. Figure 6c shows the results from our histological analysis of myelin content in the corpus callosum, cingulum, and cortex. We measured a baseline myelin area fraction of 0.73 ± 0.01 in the corpus callosum, 0.59 ± 0.04 in the cingulum, and 0.19 ± 0.08 in the cortex. In general, cortical tissue has the lowest myelin content and the corpus callosum has the highest which agrees with known neuroanatomy. In the corpus callosum, cuprizone treatment causes a significant decrease in myelin content during the first 5 weeks compared to the untreated mice. At week 6, however, we recover 84% of the baseline myelin fraction. In the cingulum, myelin content decreases during the first 4 weeks as well, but spontaneously recovers to 68% and 70% of the initial myelin fraction by weeks 5 and 6, respectively. In the cortex, myelin content drops by 19% within the first three weeks compared to baseline myelin fraction and remains stable in subsequent weeks. Despite differences in the evaluation method, our data qualitatively matches previous works very well [42,43]. More specifically, Fig. 6d shows the data reported by Gudi et al. who used proteolipid protein (PLP) immunostaining to obtain a myelin score for the corpus

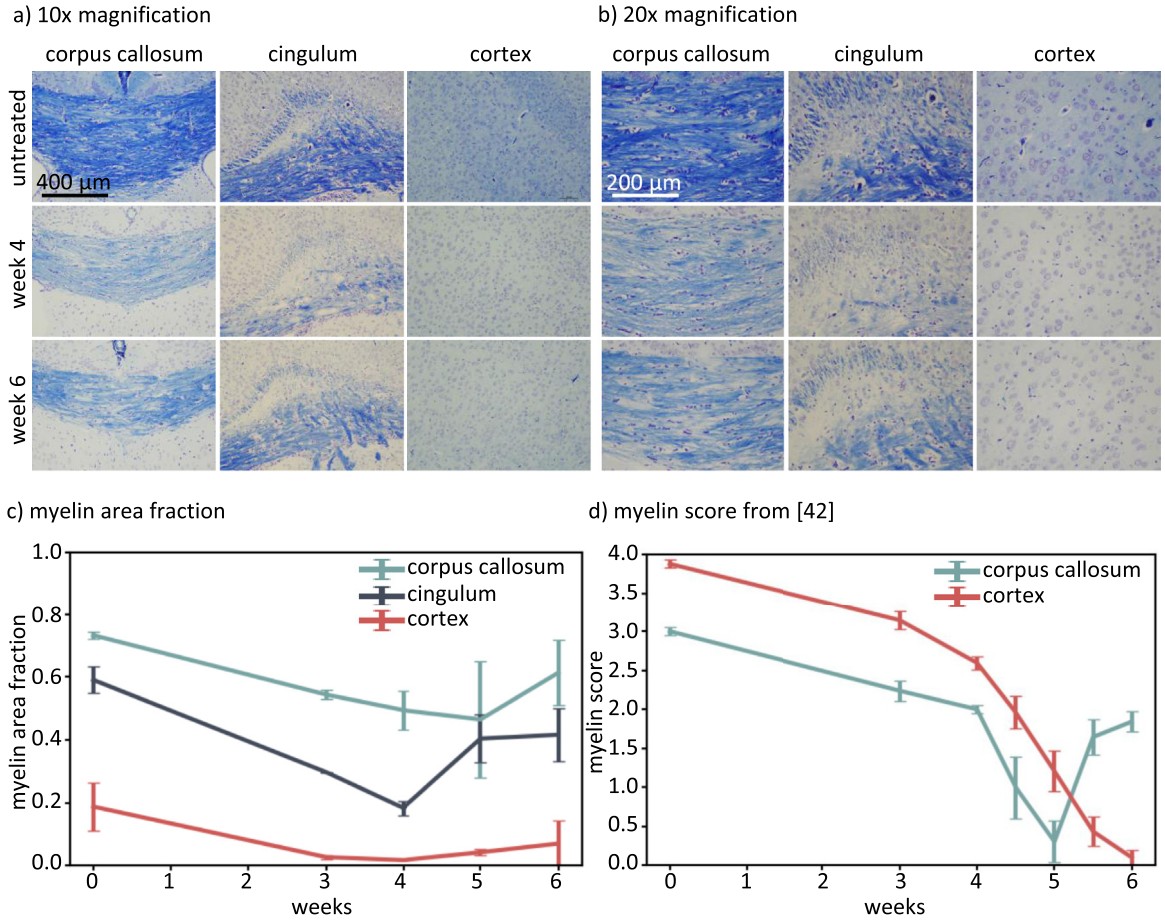

Fig. 6. Representative histological images at a) 10x and b) 20x magnification of the corpus callosum, cingulum, and cortex at baseline and at 4 and 6 weeks of cuprizone treatment, respectively (images are shown prior to undergoing image analysis to determine myelin area fraction). c) Histology-derived myelin area fraction in the corpus callosum, cingulum, and cortex at weeks 0, 3, 4, 5, and 6. d) Data from Gudi et al. who evaluated degree of myelination based on a 3-scale myelin score for the corpus callosum and a 4-scale myelin score for the cortex [42].

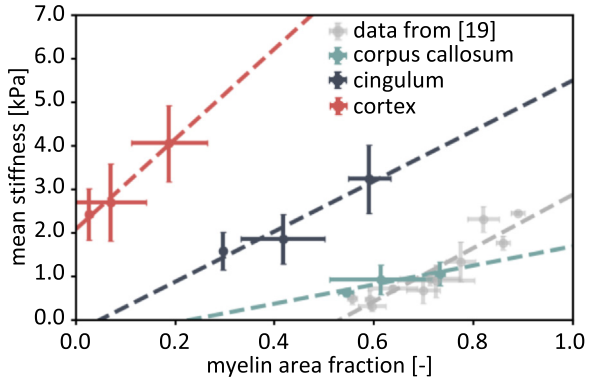

Fig. 7. Spatial correlation between myelin fraction and tissue stiffness. Each point reflects mean myelin fraction and stiffness; horizontal bars indicate standard deviation of the myelin fraction and vertical bars indicate standard deviation of the stiffness. The dashed lines indicate the linear regression of the data points for the three regions, respectively. Gray data points are from previous work by Weickenmeier et al. [19]. Results from the linear regression are summarized in Tab. 4.

callosum and cortex for the first six weeks of cuprizone treatment [42]. In the corpus callosum, they observe a gradual decrease in the myelin score of 90% within 5 weeks and a subsequent score increase of 51% by week 6. In the cortex, they observe a continuous score decrease by a total of 97% by the end of 6 weeks.

Table 4
Summary of the linear regression that maps averaged stiffness against averaged myelin area fraction for each of the three regions of interest and data previously reported by Weickenmeier et al. [19].

brain region	slope	intercept	R^2	p-value	SE [-]
corpus callosum	2.19	-0.50	0.88	0.22	0.81
cingulum	5.77	-0.27	0.93	0.17	1.57
cortex	10.35	2.09	0.99	0.07	1.08
data from [19]	6.12	-3.24	0.85	<0.001	0.84

Figure 7 maps averaged tissue stiffness against myelin fraction for the corpus callosum, cingulum, and cortex, respectively. We performed linear regression to quantify the relationship for each region and summarize the results in Table 4. We observe distinctly different trends for the three regions of interest with the highest R^2 value for the cortex ($R^2 = 0.99$), followed by the cingulum ($R^2 = 0.93$) and corpus callosum ($R^2 = 0.88$). Although the vertical offset between the trend lines suggests that local myelin content does not uniformly predict tissue stiffness across the whole brain, it is a reliable indicator for local stiffness, nonetheless. In addition, Fig. 7 also shows previously reported data from Weickenmeier et al. (gray data points) who used a similar approach to explore the relationship between white matter stiffness and myelin area fraction in pre- and post-natal bovine brains [19]. Their data shows significant overlap with the new findings reported here.

4. Discussion

The present study explores local mechanical stiffness changes in mouse brains in response to varying degrees of myelination. In the following, we discuss stiffness variations with respect to location, degree of myelination, and the difference between fresh and fixed tissue samples.

4.1. Regional stiffness differences in the mouse brain

We observe that the cortex is significantly stiffer than both the corpus callosum and cingulum with $p < 0.001$ and $p < 0.001$, respectively. Based on a total of 2055 indentation measurements, the cortex has a mean stiffness of 4.2 ± 1.3 kPa ($n = 533$) in comparison to an averaged white matter, i.e. corpus callosum and cingulum combined, stiffness of 1.9 ± 1.2 kPa ($n = 1522$) which are values comparable to measurements by Koser et al.[44]. Mouse brain stiffness, reported as the initial shear modulus derived from force-relaxation experiments, was shown to vary between 2675 ± 54 Pa in the thalamus, 2996 ± 58 Pa in the cerebellum, 4221 ± 65 Pa in the medulla, 6507 ± 65 Pa in the cortex, and 8143 ± 88 Pa in the pons, respectively [45]. Depth-controlled indentation viscoelasticity maps of mouse cortex and hippocampus show significant region-specific stiffness variations with storage moduli of around 2000 Pa and 2800 Pa, respectively[46]. Indentation measurements in the *rat cerebellum*, which use a slightly smaller indentation sphere of 40 µm and indentation depths up to 4 µm suggest effective elastic moduli of 294 ± 74 Pa in white matter and 454 ± 53 Pa in gray matter [47]. Interestingly, rat and mouse gray matter is consistently stiffer than white matter in comparison to larger animals and humans [10,12]. For example, *porcine brain* has an initial stiffness in gray matter of 731 ± 75 Pa and 3939 ± 699 Pa in white matter [48], bovine brain has average gray and white matter stiffnesses of 0.68 ± 0.2 kPa and 1.33 ± 0.64 kPa, respectively [19], and for human tissue white matter is 39% stiffer than gray matter with elastic moduli of 1.895 ± 0.6 kPa and 1.389 ± 0.29 kPa, respectively [49]. Extensive work has gone into rationalizing stiffness variations based on microstructural composition. It is repeatedly reported that tissue regions with higher nuclear density appear to be softer than tissues with lower nuclear density [9,44,46,50]. Stiffness also varies proportionally with myelin content [14,15] and decreases with proteoglycan density [6]. Proteoglycans appear in the extracellular matrix, plasma membrane of cells, and intracellular structures and regulate many cellular processes such as adhesion, proliferation, migration, differentiation, and apoptosis [50]. When we measured gray and white matter stiffness variations in untreated mice during our six week observation period, we noticed only minimal variations in each region, see Figs. 4a/c/e. This observation agrees with measurements by Guo et al. that quantified brain stiffness changes during brain maturation [51]. The regions we studied here experience marginal changes due to fully matured, stable microstructure. The other major observation is that regional stiffness differences persist during cuprizone treatment, see Figs. 4b/d/f.

4.2. Partial remyelination at week six in the corpus callosum but not the cortex

Figure 6 shows the temporal changes in myelin content due to myelin protein degradation and partial re-expression in the corpus callosum, cingulum, and cortex, respectively. Cuprizone treatment leads to a dynamic interplay between apoptotic loss of oligodendroglial cells, astrogliosis, and microgliosis and strongly varies for individual brain regions [27]. In agreement with previous work, we observe partial remyelination between weeks 4 and 6 despite continued cuprizone treatment [26,43,52,53]. Generally, myelin recovery is much more pronounced in the corpus callosum and cingulum in comparison to the cortex. These regional discrepancies are likely the result of differences in tissue structure of the myelin-rich corpus callosum and the myelin-sparse cortex [42]. In healthy mice, density of mature oligodendrocytes is much higher in the corpus callosum in comparison to the cortex. Oligodendrocyte progenitor cells (OPCs), however, are widely distributed in all brain structures including corpus callosum and cortex. Within 3 weeks of cuprizone treatment, mature oligodendrocytes are severely depleted across the whole brain [26]; the corpus callosum is broadly affected by activated microglia while the cortex only shows few scattered activated microglial cells [54]; and astrogliosis is prominent in both cortex and corpus callosum [42,55]. These noticeable variations in cellular response are reflected in the temporal and spatial differences with respect to partial remyelination. After 4.5 weeks of cuprizone treatment, oligodendrocytes reappear in white matter structures while density of adult oligodendrocytes in the cortex remains at a significantly lower level [56]. OPCs repopulate both white and gray matter structures about one week later. Unlike in white matter, however, they do not lead to the same level of partial remyelination in gray matter [43,53]. It remains unclear why signals driving remyelination in the corpus callosum are weaker in the cortex or why proliferation of OPCs in the cortex is lower than in the corpus callosum. Moreover, the roles of microglia appear to be different for the corpus callosum and cortex and are considered to have both protective as well as deleterious effects on demyelination [57]. Infiltration of activated microglia is observed in both the corpus callosum and the cortex, while microgliosis is predominantly observed in the corpus callosum and substantially lower and more diffuse in the cortex [42]. Cuprizone treatment beyond the six week mark is consistently observed to lead to chronic and mostly irreversible demyelination across the brain [29,43,56,58]. In summary, it is evident that cuprizone directly impairs a variety of essential cell functions. In the long run, irrespective of temporary remyelination of the corpus callosum, cuprizone ultimately diminishes the number of mature oligodendroglia and depletes the pool of available progenitor cells across the brain. Wherever myelin is restored, the newly formed material does not necessarily match previous microstructure and axonal function- especially in the cortex [59].

4.3. Stiffness is proportional to myelin content

Despite extensive previous work, the relationship between the brain's microstructural composition and its biomechanical response remains elusive. Location, length of observation, cellular composition, as well as numerous other factors such as age, sex, and state of health have significant impact on tissue stiffness and deformation behavior [60,61]. Budday et al. fitted a one-term Ogden model to their experimental curves and correlated the shear modulus and nonlinearity constant with local tissue constituents [6]. Their findings suggest that the shear modulus is proportional to myelin content but inversely proportional to cell nuclei density and proteoglycan content; the nonlinearity constant is proportional to collagen content but inversely proportional to cell nuclei density, lipid content, and cytoplasm content [6]. Dynamic microindentation measurements in the hippocampus by Antonovaite et al. present a similar picture: the storage modulus is significantly lower in nuclei dense regions (∼ 400-800 Pa) in comparison to stiffer regions that have a high myelin content (∼ 800-1500 Pa) [9]. Guo et al. used magnetic resonance elastography to measure brain stiffness changes during brain maturation. Evolving brain microstructure ranging from myelination to accumulation of microtubular structures, cytoskeletal linkage, cell-matrix attachment, and decreasing axonal organization, are clearly reflected in gradual tissue stiffening in nearly all brain regions [51]. Most no-

tably, the similar age-driven myelin increase observed in both gray and white matter leads to a more pronounced stiffness increase in white matter in comparison to gray matter. Except for the initial tissue softening upon cuprizone treatment, this trend matches our results which show only minor gray matter stiffness changes with progressing tissue demyelination. Eberle et al. used atomic force microscopy-based indentation measurements to compare stiffness variations in cuprizone-driven demyelinated tissues against inherited hypomyelinated tissues from Shiverer mice [20]. Although several observations, including softening of the corpus callosum with progressing cuprizone treatment, are similar to our work here, they observe some critical differences. Specifically, they do not report statistically significant differences between the cortex and corpus callosum in healthy controls, and they do not observe statistically significant stiffness changes with cuprizone treatment for both the cortex and cingulum. We suggest that these differences are due to the combination of the rather low indentation depth, young age of the cuprizone-treated animals (7 weeks at the beginning of treatment), only 5 weeks of cuprizone treatment at which point 0.2% cuprizone has not induced full demyelination [26,42,53], and the location of cortical measurements which appear fairly close to the cingulum. Interestingly, Eberle et al. point out that chronically hopymyelinated brains do not show significant stiffness differences compared to age-matched healthy controls [20,62]. Schregel et al. performed in vivo magnetic resonance elastography (MRE) measurements and subsequent histology in cuprizone treated mice to evaluate brain stiffness changes as the tissue demyelinates and ECM remodels [17]. For both control and cuprizone treated mice, the brain's viscoelastic response gradually increases during the first 9 weeks irrespective of a continuous decrease of the myelin score in cuprizone mice. After an additional three weeks, the viscoelastic response stabilized in control mice, while cuprizone-treated mice experience a ∼20% drop down to a behavior similar to 3 weeks of cuprizone treatment [17]. Interestingly, Schregel et al. observe noticeable T2-weighted signal intensity changes in the corpus callosum in comparison to the thalamus which suggests spatially heterogeneous microstructural tissue changes; findings that are confirmed by histology. In untreated mice, this change is associated with brain maturation; in cuprizone treated mice, extracellular matrix is subject to loss of parenchyma, patchy accumulation of fibronectin, glycoaminoglycans, and mucopolysaccharides, and demyelination of axons [17]. Lastly, Urbanski et al. report that acutely demyelinated tissue is softer (∼ 31%) and can recover with remyelination (within ∼ 1.5kPa in comparison to initial stiffness) while chronic demyelination leads to stiffer (∼ 35%) tissue due to augmented extracellular matrix decomposition [15]. Histology revealed that stiffening was accompanied by astrogliosis indicated by elevated GFAP and vimentin staining and an accumulation of extracellular matrix components, i.e., chondroitin sulfate proteoglycans and fibronectin. It is important to note, that samples were derived from cryo-sectioned fixed brain tissue. Fixation prior to atomic force microscopy measurements significantly increases overall tissue stiffness and, as we show in Fig. 5, does not preserve interregional stiffness ratios in comparison to fresh tissue measurements. In summary, our stiffness measurements align with previous work and clearly identify myelin as one of the strongest and most reliable markers for tissue stiffness. While myelin concentration is not directly proportional to tissue stiffness across the entire brain, its local concentration proportionally affects tissue stiffness.

4.4. Tissue fixation affects interregional stiffness ratios

Fixation helps to preserve cellular architecture, composition of cells, and the spatial relationship between proteins and the cell [63]. 10% formalin, which is 3.7% formaldehyde in water with 1% methanol, is one of the most commonly used fixation solutions. When tissues are immersed in formalin, formaldehyde reacts with various functional groups of biological macromolecules in a cross-linking fashion. This process takes between 24-48 hours, depending on sample dimensions, and inherently hardens tissue components [64] and prevents tissue decomposition, putrefaction, and autolysis [63]. In the brain, our comparison between measurements using fresh and using fixed tissues leads to two main findings: for one, fixation significantly increases average brain stiffness by a factor of 3.0 ($p < 0.001$); for the other, fixation significantly changes the stiffness ratio between the cortex and corpus callosum when comparing fixed treated mice with all other groups, i.e., fresh untreated, fresh treated, and fixed untreated mice, see Fig. 5 and Tab. 2. Additionally, the only other significant difference is the stiffness ratio between the cingulum and corpus callosum when comparing fresh untreated with fixed treated mice. All other comparisons show no difference. This implies that fixation affects the cortex differently than the corpus callosum. Urbanski et al. reported an average fixed corpus callosum stiffness of 12.07 kPa in control mice which is 3.0 times stiffer than our averaged fixed control mouse measurements [15]. Moreover, they report a ∼ 31% softening after 6 weeks of cuprizone treatment in fixed samples while we observe 2.5% stiffening in our fixed and 19.6% softening in our fresh samples. At the same time, we observed that the cingulum softens by 34.5% in fresh samples and 38.4% in fixed samples and the cortex softens by 35.7% in fresh and 43.8% in fixed samples. Taken together, there is growing evidence that fixed samples don't accurately reflect in vivo tissue property changes due to neurodegeneration. Iwashita et al. used atomic force microscopy (20 µm bead, 10 nN indentation force) to measure brain stiffness of amniotes at various maturation stages and investigated the difference between fresh tissue samples and samples fixed in either 3% glyoxal or 4% paraformaldehyde solution based on 4 week-old juvenile mice [4]. While both fixation solutions were observed to preserve overall brain structure except for minor tissue shrinkage, most glyoxal-fixed brain regions were roughly 3-times stiffer than fresh tissues and most paraformaldehyde-fixed brain regions were roughly 10-times stiffer than fresh tissues. Interestingly, they observe that the corpus callosum shows less stiffening upon fixation, i.e., a factor of ∼ 2.5 for glyoxal-based and ∼ 3.53 for paraformaldehyde-based fixation. This matches our measurements in the corpus callosum for which we obtained a factor of 3.3 upon paraformaldehyde-based fixation. More importantly, however, Iwashita et al.'s measurements indicate that interregional stiffness ratios, i.e., relative stiffness differences between the subventricular, ventricular, and intermediate zone as well as the cortical plate, are better preserved using glyoxal fixation in comparison to paraformaldehyde fixation. That said, they do not observe consistently higher or lower relative stiffness ratios for either fixation solution which suggests that individual regions respond to fixation differently. Iwashita et al. hypothesize that regions with lipid-rich myelin structures might affect cross-linking of fixatives which explains why our stiffness ratios between fixed and fresh samples are higher in the cortex (3.6) than in the corpus callosum (3.3) and cingulum (2.9) [4].

4.5. Limitations

The present work is not without limitations. First, we only measure regional stiffness on regular grids rather than assessing white matter stiffness in the entire corpus callosum or various cortical locations, respectively. Even though we observe stiffness changes with progressing cuprizone treatment in our measurements, it is likely that cuprizone-treatment affects individual subregions in the corpus callosum and cortex differently, especially with respect to spontaneous remyelination. Secondly, our histology-based myelin quantification approach compares myelin fraction from sev-

eral different slices. Given that each slice's stain intensity turns out slightly differently, comparison of absolute myelin area fraction from multiple sections may be impacted by slide preparation artefacts. Additionally, our histological analysis focused on myelin and did not include markers for other effects caused by cuprizone treatment such as neuroinflammation, astrogliosis, and depletion of oligodendrocyte progenitor cells. Future work should investigate their impact on tissue stiffness to compliment the knowledge generated in the present work. Lastly, conclusion from this mouse-based study may not extend to the human brain. Unlike in mice, for example, human white matter tissue is typically stiffer than gray matter [65].

A note on the use of contact lens solution: Due to our indentation machines layout, our indenter tip is not fully submerged such that parts of the tip enter and exit the fluid during each indentation test, see Fig. 2g. Therefore, we use a surfactant solution (here: Opti-Free contact lens solution from Alcon, Fort Worth, Texas) over established biological buffer solutions to minimize the adhesion forces between tip and fluid [66]. While this approach ensures repeatable indentation grid measurements, it cannot be excluded that prolonged surfactant exposure may damage the lipid membrane of cells [67,68]. Given the significant variations in lipid contents across cortical tissues (78-81% in myelin, 49-66% in white matter, and 36-40% in gray matter [69]), our inter-regional stiffness comparisons in sections 4.1 and 4.4 may be affected. Therefore, indentation devices that are compatible with established buffer solutions have an inherent advantage.

5. Conclusion

The cuprizone mouse model allowed us to study the impact of myelin-content on tissue stiffness at various stages during our 15-week demyelination observation period. Previously reported cuprizone-related myelin density changes, including demyelination followed by spontaneous remyelination despite continued cuprizone treatment, are closely reflected in our stiffness measurements. Although the vertical offset between the trend lines mapping mean stiffness against myelin area fraction in each region suggests that local myelin content does not uniformly predict tissue stiffness across the whole brain, it is a reliable indicator for local stiffness, nonetheless. Moreover, we establish that tissue fixation does not only significantly increase tissue stiffness, but also, more importantly, alters interregional stiffness ratios. Therefore, tissue fixation prior to mechanical characterization is an unsuitable approach to quantify realistic mechanical brain tissue properties.

Author Contributions

XZ and JW designed this study, XZ carried out the experiments, XZ and JW analyzed the data, XZ prepared the figures, and XZ and JW wrote the manuscript.

Funding

This study was supported by the National Science Foundation under grant number 1953323 to Johannes Weickenmeier.

Declaration of Competing Interest

The authors declare that the research was conducted in the absence of any commercial or financial relationships that could be construed as a potential conflict of interest.

The authors declare that they have no known competing financial interests or personal relationships that could have appeared to influence the work reported in this paper.

Supplementary material

Supplementary material associated with this article can be found, in the online version, at 10.1016/j.actbio.2023.08.033

References

[1] M.C. Murphy, G.L. Curran, K.J. Glaser, P.J. Rossman, J. Huston III, J.F. Poduslo, C.R. Jack Jr, J.P. Felmlee, R.L. Ehman, Magnetic resonance elastography of the brain in a mouse model of alzheimer's disease: initial results, Magnetic resonance imaging 30 (2012) 535–539.
[2] C. Klein, E.G. Hain, J. Braun, K. Riek, S. Mueller, B. Steiner, I. Sack, Enhanced adult neurogenesis increases brain stiffness: in vivo magnetic resonance elastography in a mouse model of dopamine depletion, PloS one 9 (2014) e92582.
[3] S. Budday, G. Sommer, C. Birkl, C. Langkammer, J. Haybaeck, J. Kohnert, M. Bauer, F. Paulsen, P. Steinmann, E. Kuhl, G.A. Holzapfel, Mechanical characterization of human brain tissue, Acta biomaterialia 48 (2017) 319–340.
[4] M. Iwashita, T. Nomura, T. Suetsugu, F. Matsuzaki, S. Kojima, Y. Kosodo, Comparative analysis of brain stiffness among amniotes using glyoxal fixation and atomic force microscopy, Frontiers in cell and developmental biology 8 (2020) 574619.
[5] L.V. Hiscox, C.L. Johnson, M.D. McGarry, H. Marshall, C.W. Ritchie, E.J.V. Beek, N. Roberts, J.M. Starr, Mechanical property alterations across the cerebral cortex due to alzheimer's disease, Brain communications 2 (2020) fcz049.
[6] S. Budday, M. Sarem, L. Starck, G. Sommer, J. Pfefferle, N. Phunchago, E. Kuhl, F. Paulsen, P. Steinmann, V. Shastri, G. Holzapfel, Towards microstructure-informed material models for human brain tissue, Acta Biomaterialia 104 (2020) 53–65.
[7] K. Linka, N. Reiter, J. Würges, M. Schicht, L. Bräuer, C.J. Cyron, F. Paulsen, S. Budday, Unraveling the local relation between tissue composition and human brain mechanics through machine learning, Frontiers in bioengineering and biotechnology 9 (2021) 704738.
[8] N. Reiter, B. Roy, F. Paulsen, S. Budday, Insights into the microstructural origin of brain viscoelasticity, Journal of Elasticity 145 (2021) 99–116.
[9] N. Antonovaite, L.A. Hulshof, E.M. Hol, W.J. Wadman, D. Iannuzzi, Viscoelastic mapping of mouse brain tissue: relation to structure and age, journal of the mechanical behavior of biomedical materials 113 (2021) 104159.
[10] S. Budday, G. Sommer, J. Haybaeck, P. Steinmann, G.A. Holzapfel, E. Kuhl, Rheological characterization of human brain tissue, Acta biomaterialia 60 (2017) 315–329.
[11] J. Weickenmeier, M. Kurt, E. Ozkaya, M. Wintermark, K.B. Pauly, E. Kuhl, Magnetic resonance elastography of the brain: a comparison between pigs and humans, Journal of the mechanical behavior of biomedical materials 77 (2018) 702–710.
[12] D.B. MacManus, A. Menichetti, B. Depreitere, N. Famaey, J.V. Sloten, M. Gilchrist, Towards animal surrogates for characterising large strain dynamic mechanical properties of human brain tissue, Brain Multiphysics 1 (2020) 100018.
[13] J.V. Dommelen, T.V.d. Sande, M. Hrapko, G. Peters, Mechanical properties of brain tissue by indentation: interregional variation, Journal of the mechanical behavior of biomedical materials 3 (2010) 158–166.
[14] J. Weickenmeier, R. de Rooij, S. Budday, P. Steinmann, T.C. Ovaert, E. Kuhl, Brain stiffness increases with myelin content, Acta biomaterialia 42 (2016) 265–272.
[15] M.M. Urbanski, M.B. Brendel, C.V. Melendez-Vasquez, Acute and chronic demyelinated cns lesions exhibit opposite elastic properties, Scientific reports 9 (2019) 1–13.
[16] S. Cheng, E.C. Clarke, L.E. Bilston, Rheological properties of the tissues of the central nervous system: a review, Medical engineering & physics 30 (2008) 1318–1337.
[17] K. Schregel, E.W.n. Tysiak, P. Garteiser, I. Gemeinhardt, T. Prozorovski, O. Aktas, H. Merz, D. Petersen, J. Wuerfel, R. Sinkus, Demyelination reduces brain parenchymal stiffness quantified in vivo by magnetic resonance elastography, Proceedings of the National Academy of Sciences 109 (2012) 6650–6655.
[18] J. Schmidt, D. Tweten, A. Badachhape, A. Reiter, R. Okamoto, J. Garbow, P. Bayly, Measurement of anisotropic mechanical properties in porcine brain white matter ex vivo using magnetic resonance elastography, Journal of the mechanical behavior of biomedical materials 79 (2018) 30–37.
[19] J. Weickenmeier, R. de Rooij, S. Budday, T.C. Ovaert, E. Kuhl, The mechanical importance of myelination in the central nervous system, Journal of the mechanical behavior of biomedical materials 76 (2017) 119–124.
[20] D. Eberle, G. Fodelianaki, T. Kurth, A. Jagielska, S. Möllmert, E. Ulbricht, K. Wagner, A.V. Taubenberger, N. Träber, J.-C. Escolano, K.V. Vliet, Acquired demyelination but not genetic developmental defects in myelination leads to brain tissue stiffness changes, Brain Multiphysics 1 (2020) 100019.
[21] N. Antonovaite, L.A. Hulshof, C.F. Huffels, E.M. Hol, W.J. Wadman, D. Iannuzzi, Mechanical alterations of the hippocampus in the app/ps1 alzheimer's disease mouse model, Journal of the Mechanical Behavior of Biomedical Materials 122 (2021) 104697.
[22] K. Franze, P.A. Janmey, J. Guck, Mechanics in neuronal development and repair, Annual review of biomedical engineering 15 (2013) 227–251.
[23] S. Möllmert, M.A. Kharlamova, T. Hoche, A.V. Taubenberger, S. Abuhattum, V. Kuscha, T. Kurth, M. Brand, J. Guck, Zebrafish spinal cord repair is accompanied by transient tissue stiffening, Biophysical journal 118 (2020) 448–463.

[24] J.N. Giedd, J. Blumenthal, N.O. Jeffries, F.X. Castellanos, H. Liu, A. Zijdenbos, T. Paus, A.C. Evans, J.L. Rapoport, Brain development during childhood and adolescence: a longitudinal mri study, Nature neuroscience 2 (1999) 861–863.
[25] B.F.G. Popescu, C.F. Lucchinetti, Pathology of demyelinating diseases, Annual Review of Pathology: Mechanisms of Disease 7 (2012) 185–217.
[26] M. Kipp, T. Clarner, J. Dang, S. Copray, C. Beyer, The cuprizone animal model: new insights into an old story, Acta neuropathologica 118 (2009) 723–736.
[27] J. Praet, C. Guglielmetti, Z. Berneman, A.V.d. Linden, P. Ponsaerts, Cellular and molecular neuropathology of the cuprizone mouse model: clinical relevance for multiple sclerosis, Neuroscience & Biobehavioral Reviews 47 (2014) 485–505.
[28] M. Zirngibl, P. Assinck, A. Sizov, A.V. Caprariello, J.R. Plemel, Oligodendrocyte death and myelin loss in the cuprizone model: an updated overview of the intrinsic and extrinsic causes of cuprizone demyelination, Molecular Neurodegeneration 17 (2022) 1–28.
[29] A.J. Steelman, J.P. Thompson, J. Li, Demyelination and remyelination in anatomically distinct regions of the corpus callosum following cuprizone intoxication, Neuroscience research 72 (2012) 32–42.
[30] Y. Blinkouskaya, J. Weickenmeier, Brain shape changes associated with cerebral atrophy in healthy aging and alzheimer's disease, Frontiers in Mechanical Engineering (2021) 64.
[31] V.L. Visser, H. Rusinek, J. Weickenmeier, Peak ependymal cell stretch overlaps with the onset locations of periventricular white matter lesions, Scientific Reports 2021 11:1 11 (2021) 1–12.
[32] A. Caçoilo, H. Rusinek, J. Weickenmeier, 3d finite-element brain modeling of lateral ventricular wall loading to rationalize periventricular white matter hyperintensity locations, Engineering with Computers 38 (2022) 3939–3955.
[33] J. Weickenmeier, E. Kuhl, A. Goriely, Multiphysics of prionlike diseases: Progression and atrophy, Physical review letters 121 (2018) 158101.
[34] W. Brück, A. Bitsch, H. Kolenda, Y. Brück, M. Stiefel, H. Lassmann, Inflammatory central nervous system demyelination: correlation of magnetic resonance imaging findings with lesion pathology, Annals of neurology 42 (1997) 783–793.
[35] E. Sechi, K.N. Krecke, S.A. Messina, M. Buciuc, S.J. Pittock, J.J. Chen, B.G. Weinshenker, A.S. Lopez-Chiriboga, C.F. Lucchinetti, N.L. Zalewski, Comparison of mri lesion evolution in different central nervous system demyelinating disorders, Neurology 97 (2021) e1097–e1109.
[36] C.L. Johnson, M.D. McGarry, A.A. Gharibans, J.B. Weaver, K.D. Paulsen, H. Wang, W.C. Olivero, B.P. Sutton, J.G. Georgiadis, Local mechanical properties of white matter structures in the human brain, Neuroimage 79 (2013) 145–152.
[37] Q. Wang, S.-L. Ding, Y. Li, J. Royall, D. Feng, P. Lesnar, N. Graddis, M. Naeemi, B. Facer, A. Ho, et al., The allen mouse brain common coordinate framework: a 3d reference atlas, Cell 181 (2020) 936–953.
[38] I.N. Sneddon, The relation between load and penetration in the axisymmetric boussinesq problem for a punch of arbitrary profile, International journal of engineering science 3 (1965) 47–57.
[39] S.R. Bodhireddy, W.D. Lyman, W.K. Rashbaum, K.M. Weidenheim, Immunohistochemical detection of myelin basic protein is a sensitive marker of myelination in second trimester human fetal spinal cord, Journal of Neuropathology & Experimental Neurology 53 (1994) 144–149.
[40] P.A. Humphrey, L.P. Dehner, J.D. Pfeifer, The Washington manual of surgical pathology, Lippincott Williams & Wilkins, 2008.
[41] J. Weickenmeier, R. de Rooij, S. Budday, P. Steinmann, T. Ovaert, E. Kuhl, Brain stiffness increases with myelin content, Acta Biomaterialia 42 (2016) 265–272.
[42] V. Gudi, D. Moharregh-Khiabani, T. Skripuletz, P.N. Koutsoudaki, A. Kotsiari, J. Skuljec, C. Trebst, M. Stangel, Regional differences between grey and white matter in cuprizone induced demyelination, Brain research 1283 (2009) 127–138.
[43] G.K. Matsushima, P. Morell, The neurotoxicant, cuprizone, as a model to study demyelination and remyelination in the central nervous system, Brain pathology 11 (2001) 107–116.
[44] D.E. Koser, E. Moeendarbary, J. Hanne, S. Kuerten, K. Franze, Cns cell distribution and axon orientation determine local spinal cord mechanical properties, Biophysical journal 108 (2015) 2137–2147.
[45] D.B. MacManus, B. Pierrat, J.G. Murphy, M.D. Gilchrist, A viscoelastic analysis of the p56 mouse brain under large-deformation dynamic indentation, Acta Biomaterialia 48 (2017) 309–318.
[46] N. Antonovaite, S.V. Beekmans, E.M. Hol, W.J. Wadman, D. Iannuzzi, Regional variations in stiffness in live mouse brain tissue determined by depth-controlled indentation mapping, Scientific Reports 8 (2018) 1–11.
[47] A.F. Christ, K. Franze, H. Gautier, P. Moshayedi, J. Fawcett, R.J. Franklin, R.T. Karadottir, J. Guck, Mechanical difference between white and gray matter in the rat cerebellum measured by scanning force microscopy, Journal of biomechanics 43 (2010) 2986–2992.
[48] B.S. Elkin, A. Ilankova, I.M. Barclay, Dynamic, regional mechanical properties of the porcine brain: Indentation in the coronal plane, Journal of Biomechanical Engineering 133 (2011).
[49] S. Budday, R. Nay, R. de Rooij, P. Steinmann, T. Wyrobek, T.C. Ovaert, E. Kuhl, Mechanical properties of gray and white matter brain tissue by indentation, Journal of the mechanical behavior of biomedical materials 46 (2015) 318–330.
[50] C. Zhang, C. Liu, H. Zhao, Mechanical properties of brain tissue based on microstructure, Journal of the Mechanical Behavior of Biomedical Materials (2021) 104924.
[51] J. Guo, G. Bertalan, D. Meierhofer, C. Klein, S. Schreyer, B. Steiner, S. Wang, R.V.d. Silva, C. Infante-Duarte, S. Koch, P. Boehm-Sturm, J. Braun, I. Sack, Brain maturation is associated with increasing tissue stiffness and decreasing tissue fluidity, Acta Biomaterialia 99 (2019) 433–442.
[52] X. Gao, T.A. Gillig, P. Ye, A.J. D'Ercole, G.K. Matsushima, B. Popko, Interferon-γ protects against cuprizone-induced demyelination, Molecular and Cellular Neuroscience 16 (2000) 338–349.
[53] M. Lindner, S. Heine, K. Haastert, N. Garde, J. Fokuhl, F. Linsmeier, C. Grothe, W. Baumgärtner, M. Stangel, Sequential myelin protein expression during remyelination reveals fast and efficient repair after central nervous system demyelination, Neuropathology and applied neurobiology 34 (2008) 105–114.
[54] V. Gudi, S. Gingele, T. Skripuletz, M. Stangel, Glial response during cuprizone-induced de-and remyelination in the cns: lessons learned, Frontiers in cellular neuroscience 8 (2014) 73.
[55] N. Hibbits, J. Yoshino, T.Q. Le, R.C. Armstrong, Astrogliosis during acute and chronic cuprizone demyelination and implications for remyelination, ASN neuro 4 (2012) AN20120062.
[56] L.-A. Harsan, J. Steibel, A. Zaremba, A. Agin, R. Sapin, P. Poulet, B. Guignard, N. Parizel, D. Grucker, N. Boehm, R. Miller, M.S. Ghandour, Recovery from chronic demyelination by thyroid hormone therapy: myelinogenesis induction and assessment by diffusion tensor magnetic resonance imaging, Journal of Neuroscience 28 (2008) 14189–14201.
[57] T. Skripuletz, D. Hackstette, K. Bauer, V. Gudi, R. Pul, E. Voss, K. Berger, M. Kipp, W. Baumgärtner, M. Stangel, Astrocytes regulate myelin clearance through recruitment of microglia during cuprizone-induced demyelination, Brain 136 (2013) 147–167.
[58] J.M. Vega-Riquer, G. Mendez-Victoriano, R.A. Morales-Luckie, O. Gonzalez-Perez, Five decades of cuprizone, an updated model to replicate demyelinating diseases, Current neuropharmacology 17 (2019) 129–141.
[59] J. Orthmann-Murphy, C.L. Call, G.C. Molina-Castro, Y.C. Hsieh, M.N. Rasband, P.A. Calabresi, D.E. Bergles, Remyelination alters the pattern of myelin in the cerebral cortex, Elife 9 (2020) e56621.
[60] C.M. Hall, E. Moeendarbary, G.K. Sheridan, Mechanobiology of the brain in ageing and alzheimer's disease, European Journal of Neuroscience 53 (2021) 3851–3878.
[61] S. Budday, T.C. Ovaert, G.A. Holzapfel, P. Steinmann, E. Kuhl, Fifty shades of brain: a review on the mechanical testing and modeling of brain tissue, Archives of Computational Methods in Engineering 27 (2020) 1187–1230.
[62] A. Jagielska, A.L. Norman, G. Whyte, K.J.V. Vliet, J. Guck, R.J. Franklin, Mechanical environment modulates biological properties of oligodendrocyte progenitor cells, Stem cells and development 21 (2012) 2905–2914.
[63] R. Thavarajah, V.K. Mudimbaimannar, J. Elizabeth, U.K. Rao, K. Ranganathan, Chemical and physical basics of routine formaldehyde fixation, Journal of oral and maxillofacial pathology: JOMFP 16 (2012) 400.
[64] S.-J. Estermann, S. Förster-Streffleur, L. Hirtler, J. Streicher, D.H. Pahr, A. Reisinger, Comparison of thiel preserved, fresh human, and animal liver tissue in terms of mechanical properties, Annals of Anatomy-Anatomischer Anzeiger 236 (2021) 151717.
[65] I. Sack, K.-J. Streitberger, D. Krefting, F. Paul, J. Braun, The influence of physiological aging and atrophy on brain viscoelastic properties in humans, PLoS ONE 6 (2011) e23451.
[66] J.C. Kohn, D.M. Ebenstein, Eliminating adhesion errors in nanoindentation of compliant polymers and hydrogels, Journal of the mechanical behavior of biomedical materials 20 (2013) 316–326.
[67] H. Heerklotz, Interactions of surfactants with lipid membranes, Quarterly reviews of biophysics 41 (2008) 205–264.
[68] C.K. Postnikoff, R. Pintwala, S. Williams, A.M. Wright, D. Hileeto, M.B. Gorbet, Development of a curved, stratified, in vitro model to assess ocular biocompatibility, PloS one 9 (2014) e96448.
[69] J.S. O'Brien, E.L. Sampson, Lipid composition of the normal human brain: gray matter, white matter, and myelin, Journal of lipid research 6 (1965) 537–544.

Supplementary Materials:
Brain Stiffness Follows Cuprizone-Induced Variations in Local Myelin Content

S.1. Summary of all indentation measurements based on fresh tissue samples

In Fig. S1, we show the stiffness of every single indentation measurement where we plot measurements from the same animal with the same color.

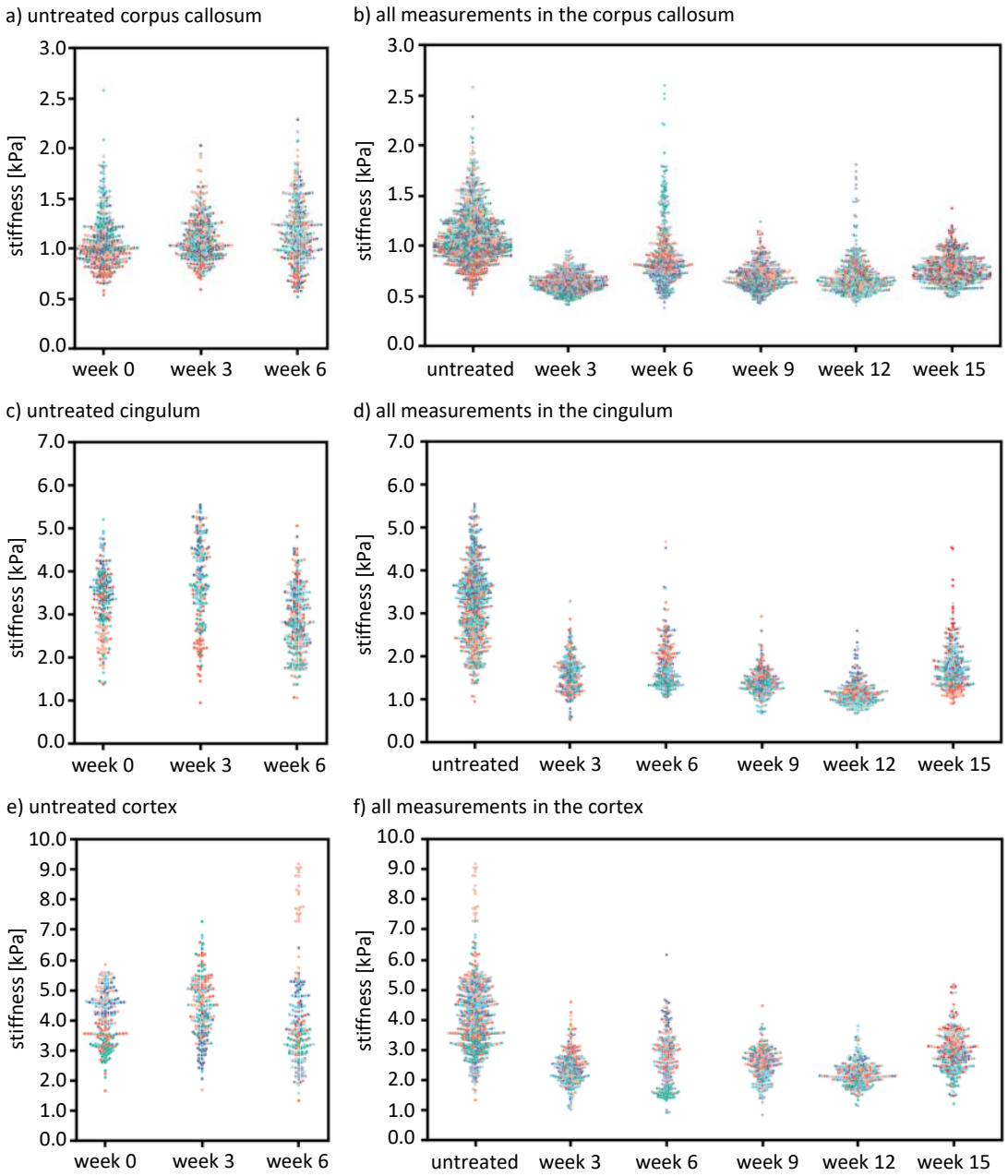

Figure S1: Stiffness of every single indentation measurement. For each week, measurements from the same animal have the same color. We report data for untreated animals at weeks 0, 3, and 6 in the a) corpus callosum, c) cingulum, and e) cortex. b/d/f show data from treated mice in comparison to all untreated data bundles together.

S.2. Summary of all indentation measurements used for the fresh-fixed measurement comparison

In Fig. S2, we show the stiffness value of every single indentation used for the fresh-fixed measurement comparison. We differentiate between untreated and treated measurements at observation week 6.

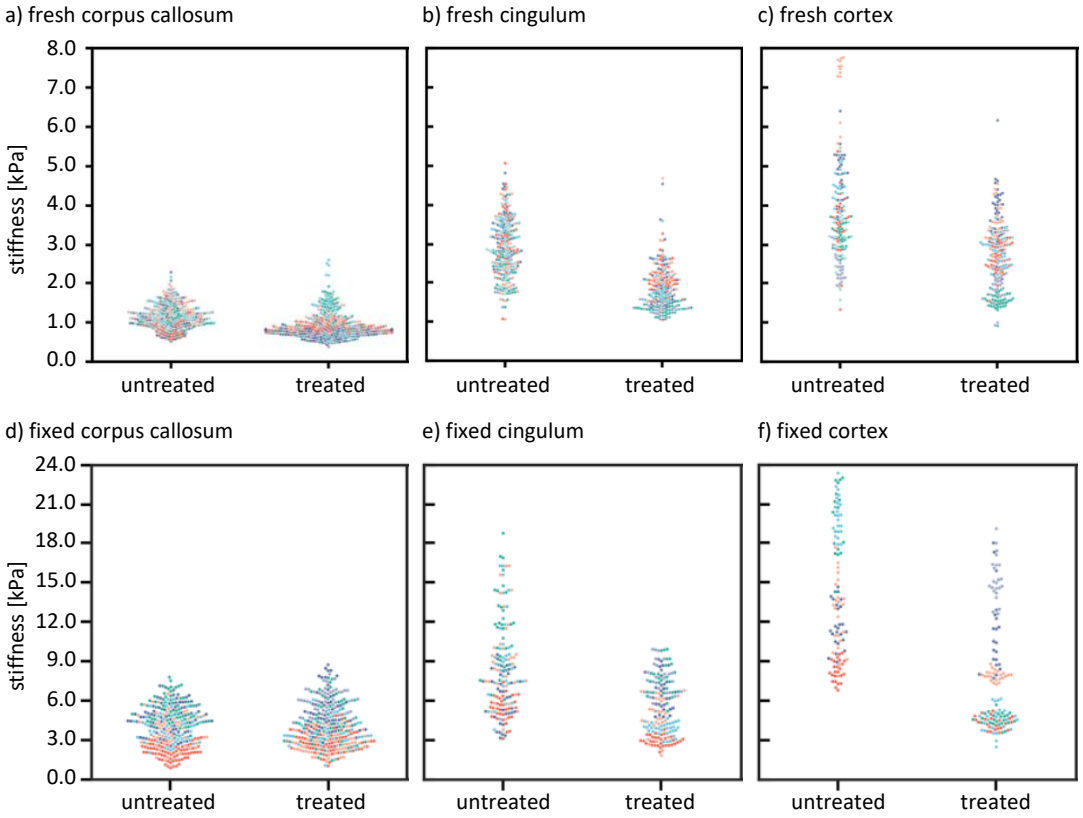

Figure S2: Stiffness of every single indentation measurement used for the fresh and fixed comparison. For the corpus callosum, cingulum, and cortex, we report data for untreated and treated mice from observation week 6, respectively.

S.3. Results from the bootstrapping approach to determine interregional stiffness ratios

In Fig. S3, we summarize the results from our bootstrapping approach. For each animal, we performed 1000 iterations at which we randomly sampled 10 data points from each region. From this data, we then compute ten ratios for each of the three interregional stiffness ratios and their respective means. From the 1000 means of each interregional stiffness ratio, we construct the histograms in the figure shown below. More specifically, we ranked animals based on the cortex/corpus callosum ratio from minimum to maximum ratio. We would like to point out two considerations: (i) fixed treated mice have a substantially lower cortex/corpus callosum ratio which is reflected in the statistical significant shown in Fig. 5 and (ii) the 1000 means follow normal distributions such that we compute their means for subsequent analysis.

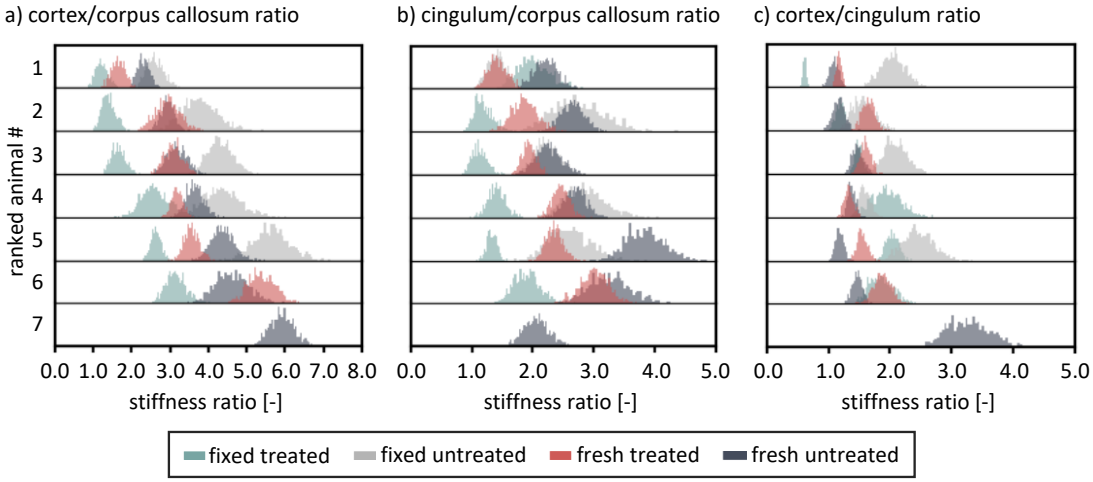

Figure S3: Summary of our bootstrapping approach. We ranked all animals' histograms based on the cortex/corpus callosum ratio from minimum to maximum value. Interestingly, we observe that this ranking visualizes the clear difference of fixed treated mice in comparison to all three other groups, i.e., fresh untreated, fresh treated, and fixed untreated for the interregional ratios that include the corpus callosum.